J|A|C|S ARTICLES

Published on Web 02/20/2009

Configurationally Rigid Pentaorganosilicates

Erik P. A. Couzijn, Daniël W. F. van den Engel, J. Chris Slootweg, Frans J. J. de Kanter, Andreas W. Ehlers, Marius Schakel, and Koop Lammertsma*

Department of Chemistry and Pharmaceutical Sciences, Faculty of Sciences, VU University Amsterdam, De Boelelaan 1083, NL-1081 HV Amsterdam, The Netherlands

Received November 23, 2008; E-mail: k.lammertsma@few.vu.nl

Abstract: The intramolecular substituent interchange in recently reported pentaorganosilicates is investigated by B3LYP calculations, which show excellent agreement with the experimental thermochemical data. Two types of ligand permutation are discerned (A and B), which both lead to racemization of the helical, spirocyclic anions. IRC calculations show that stereomutation A bifurcates into two enantiomeric reaction paths, which are inhibited by ortho substitution of the bidentate ligands. The other pathway (B) proceeds through a trigonal bipyramidal transition state with one bisequatorial bidentate ligand and is disfavored by increasing the π-electron density of the ligand. A more electronegative fifth, monodentate substituent increases the barrier of pathway A and lowers that of pathway B, as in bis(biphenyl-2,2′-diyl)fluorosilicate, which is the first tetraorganofluorosilicate to be isolated and fully characterized. These concepts enabled us to design and synthesize methyl- and ethylbis([2]naphthylpyrrol-2,1′-diyl)silicate as Si-chiral pentaorganosilicates that are configurationally rigid at room temperature.

Introduction

Hypervalent silicon compounds have received unremitting interest, and a plethora of such species has been synthesized in the past decades, most of them containing oxygen, nitrogen, and/or fluorine substituents.[1−7] The recent synthesis of the highly stable, all-carbon substituted silicates **1** and **2** (Chart 1) is illustrative of the opportunities in hypervalent silicon chemistry.[2−5] The crystal structures of **1b**, **1c**, and **2b** show these spirocyclic anions to be weakly coordinating[3,4] and to have a propeller-like shape with a left-handed (Λ) or right-handed (Δ) helix. However, in solution pentacoordinate silicon species generally undergo facile intramolecular substituent permutation via Berry pseudorotation[8] or one of the pathways suggested by Muetterties (see below).[9,10] NMR studies on **1** and **2** revealed modest stereomutational barriers of 13 and 15.5 kcal mol^{-1}, respectively,[2,4] making resolution of the racemic mixtures at room temperature impossible.

Most of the known spirocyclic silicates are multiply heterosubstituted and are based on the 1,2-benzenediolato moiety or the Martin ligand[6] ($-o$-$C_6H_4C(CF_3)_2O-$) with Si-epimerization barriers for e.g., silicates **3a**,**b** of 29 kcal mol^{-1}.[6a,b] Tacke et al.[7] reported zwitterionic silicates derived from α-hydroxycarboxylic acids and α-amino acids with stereomutational barriers of up to 21 kcal mol^{-1} for **4**. The neutral pentacoordinate phosphorus analogues show more rigidity. Hellwinkel et al.[11] reported bis(biaryl)phosphoranes with racemization barriers of

(1) Recent reviews on hypervalent silicates:(a) Chuit, C.; Corriu, R. J. P.; Reyé, C.; Young, J. C. *Chem. Rev* **1993**, *93*, 1371–1448. (b) Holmes, R. R. *Chem. Rev.* **1990**, *90*, 17–31. (c) Bassindale, A. R.; Taylor, P. G. In *The Chemistry of Organic Silicon Compounds*; Patai, S., Rappoport, Z., Eds; John Wiley & Sons Ltd.: New York, 1989; Part 1, pp 839−892. (d) Corriu, R. J. P.; Young, J. C. In *The Chemistry of Organic Silicon Compounds*; Patai, S., Rappoport, Z., Eds; John Wiley & Sons: Chichester, U.K., 1989; Part 2, pp 1241−1288.

(2) (a) de Keijzer, A. H. J. F.; de Kanter, F. J. J.; Schakel, M.; Osinga, V. P.; Klumpp, G. W. *J. Organomet. Chem.* **1997**, *548*, 29–32. (b) de Keijzer, A. H. J. F. From Dilithiomethanes to Pentaorganylsilicates, PhD Thesis, Vrije Universiteit, Amsterdam, The Netherlands, 2000; Chapter 4.

(3) (a) Deerenberg, S.; Schakel, M.; de Keijzer, A. H. J. F.; Kranenburg, M.; Lutz, M.; Spek, A. L.; Lammertsma, K. *Chem. Commun.* **2002**, 348–349. (b) Ballweg, D.; Liu, Y. X.; Guzei, I. A.; West, R. *Silicon Chem.* **2002**, *1*, 57–60.

(4) Couzijn, E. P. A.; Schakel, M.; de Kanter, F. J. J.; Ehlers, A. W.; Lutz, M.; Spek, A. L.; Lammertsma, K. *Angew. Chem., Int. Ed.* **2004**, *43*, 3440–3442.

(5) Couzijn, E. P. A.; Ehlers, A. W.; Schakel, M.; Lammertsma, K. *J. Am. Chem. Soc.* **2006**, *128*, 13634–13639.

(6) See for example:(a) Stevenson, W. H.; Wilson, S.; Martin, J. C.; Farnham, W. B. *J. Am. Chem. Soc.* **1985**, *107*, 6340–6352, and references therein. (b) Chopra, S. K.; Martin, J. C. *J. Am. Chem. Soc.* **1990**, *112*, 5342–5343. (c) Kira, M.; Sato, K.; Sakurai, H. *J. Am. Chem. Soc.* **1988**, *110*, 4599–4602. (d) Boudin, A.; Cerveau, G.; Chuit, C.; Corriu, R. J. P.; Reyé, C. *Angew. Chem., Int. Ed. Engl.* **1986**, *25*, 473–474. (e) Kumara Swamy, K. C.; Chandrasekhar, V.; Harland, J. J.; Holmes, J. M.; Day, R. O.; Holmes, R. R. *J. Am. Chem. Soc.* **1990**, *112*, 2341–2348. (f) Mercado, R.-M. L.; Chandrasekaran, A.; Day, R. O.; Holmes, R. R. *Organometallics* **1999**, *18*, 1686–1692.

(7) (a) Tacke, R.; Becht, J.; Dannappel, O.; Ahlrichs, R.; Schneider, U.; Sheldrick, W. S.; Hahn, J.; Kiesgen, F. *Organometallics* **1996**, *15*, 2060–2077. (b) Tacke, R.; Bertermann, R.; Biller, A.; Dannappel, O.; Pülm, M.; Willeke, R. *Eur. J. Inorg. Chem.* **1999**, 795–805. (c) Tacke, R.; Pfrommer, B.; Pülm, M.; Bertermann, R. *Eur. J. Inorg. Chem.* **1999**, 807–816. (d) Kost, D.; Kalikhman, I.; Krivonos, S.; Bertermann, R.; Burschka, C.; Neugebauer, R. E.; Pülm, M.; Willeke, R.; Tacke, R. *Organometallics* **2000**, *19*, 1083–1095. (e) Tacke, R.; Bertermann, R.; Biller, A.; Dannappel, O.; Penka, M.; Pülm, M.; Willeke, R. *Z. Anorg. Allg. Chem.* **2000**, *626*, 1159–1173. (f) Tacke, R.; Mallak, M.; Willeke, R. *Angew. Chem., Int. Ed.* **2001**, *40*, 2339–2341. (g) Tacke, R.; Bertermann, R.; Burschka, C.; Dragota, S.; Penka, M.; Richter, I. *J. Am. Chem. Soc.* **2004**, *126*, 14493–14505. (h) Dragota, S.; Bertermann, R.; Burschka, C.; Penka, M.; Tacke, R. *Organometallics* **2005**, *24*, 5560–5568.

(8) (a) Berry, R. S. *J. Chem. Phys.* **1960**, *32*, 933–938. (b) Berry, R. S. *Rev. Mod. Phys.* **1960**, *32*, 447–454.

(9) (a) Muetterties, E. L. *J. Am. Chem. Soc.* **1969**, *91*, 4115–4122. (b) Muetterties, E. L. *J. Am. Chem. Soc.* **1969**, *91*, 1636–1643.

Chart 1

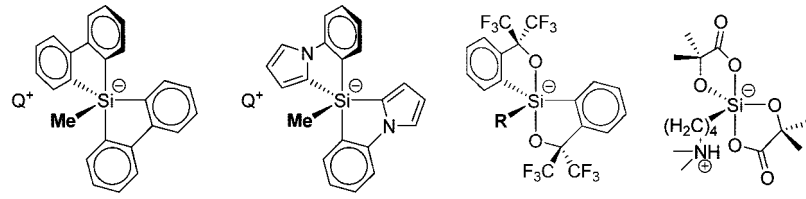

1a: $Q^+ = [Li(THF)_4]^+$ **2a**: $Q^+ = [Li(THF)_4]^+$ **3a**: R = MeCHPh **4**
b: $Q^+ = nBu_4N^+$ **b**: $Q^+ = nBu_4N^+$ **b**: R = *n*Bu
c: $Q^+ = [Li(DME)_3]^+$

up to 28 kcal mol^{-1}, whereas lately the group of Akiba[12] achieved the optical resolution of Martin-type phosphoranes.

We envisage that configurationally rigid silicates may be applicable as, e.g., chiral cocatalysts or chiral ionic liquids.[13,14] Because heteroatoms attached to silicon are prone to coordination, as in **4** that exists as hydrogen-bonded dimers in the solid state,[7c] it is desirable to design structurally rigid, stable pentaorganosilicates based on the biaryl moiety, as in **1** and **2**. Earlier we reported on the factors that determine the stability of these species.[5] Preceding ab initio studies on the stereomutation of silicates have been limited to small systems.[15] Only recently, theoretical studies were conducted on larger hetero-substituted systems, but without reaction path analyses.[7a−c,e,g] Here, we present a detailed B3LYP survey[16] on the dynamic behavior of **1** and **2** and on the newly synthesized anions **5** and **6**. We correlate these results with experimental data and address the factors that influence the barrier heights for interconversion.

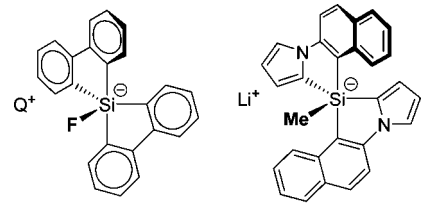

5a: $Q^+ = Cs^+$ **6**
b: $Q^+ = Me_4N^+$

Results and Discussion

We first discuss the general structure of spirocyclic bis(biaryl)silicates and the two feasible types of substituent permutation. These pathways are examined in detail for **1**, which is the simplest pentaorganosilicate that is stable in the condensed phase. The gas-phase calculations may be related to the experimental data because of the weakly coordinating nature of the silicate anions.[17] We then report on the synthesis of silicate **5**, carrying F instead of Me as the fifth, monodentate substituent, which is stable in solution up to 87 °C. To the best of our knowledge, **5** is the first tetraorganofluorosilicate to be isolated and fully characterized. Hitherto, only a few species with a SiC_4F core have been observed as reactive intermediates either in the gas phase or in solution.[18,19] Next, we analyze the complex configurational isomerism of **2**, which bears the smaller but more π-electron rich phenylpyrrole bidentate ligands, to reveal the effects of the monodentate and bidentate substituents on the stereomutational barriers. Finally, on the basis of these analyses we present the design, synthesis, and characterization of the configurationally rigid, stable pentaorganosilicate **6**.

Structure and Substituent Permutation of Bis(biaryl)silicates. Two ideal geometries are possible for pentacoordinate silicon species, namely a trigonal bipyramid (TBP) with two axial (ax) and three equatorial (eq) substituents, and a rectangular pyramid (RP) with one apical (ap) and four basal (bas) substituents. Due to the electropositive nature of silicon, its bonds are polar covalent with the negative charge distributed over the substituents.[5] The ionic character of the bonds increases

(10) The so-called turnstile rotation has also been proposed as an alternative mechanism. However, turnstile rotation is topologically indistinguishable from Berry pseudorotation and differs only by imposing artificial constraints on the transition state geometry. Therefore, turnstile rotation is rather a special realization of the Berry pseudorotation mechanism: (a) Ugi, I.; Marquarding, D.; Klusacek, H.; Gillespie, P.; Ramirez, F. *Acc. Chem. Res.* **1971**, *4*, 288–296. (b) Gillespie, P.; Hoffman, P.; Klusacek, H.; Marquarding, D.; Pfohl, S.; Ramirez, F.; Tsolis, E. A.; Ugi, I. *Angew. Chem., Int. Ed. Engl.* **1971**, *10*, 687–715. (c) Russegger, P.; Brickmann, J. *Chem. Phys. Lett.* **1975**, *30*, 276–278. (d) Altmann, J. A.; Yates, K.; Czismadia, I. G. *J. Am. Chem. Soc.* **1976**, *98*, 1450–1454. (e) Kutzelnigg, W.; Wasilewski, J. *J. Am. Chem. Soc.* **1982**, *104*, 953–960. (f) Wang, P; Agrafiotis, D. K.; Streitwieser, A.; Schleyer, P. v. R. *Chem. Commun.* **1990**, *3*, 201–203. (g) Bento, A. P.; Bickelhaupt, M. *Chem. Asian J.* **2008**, *3*, 1783–1792.

(11) (a) Hellwinkel, D.; Lindner, W.; Schmidt, W. *Chem. Ber.* **1979**, *112*, 281–291. (b) Hellwinkel, D.; Krapp, W. *Chem. Ber.* **1979**, *112*, 292–297. (c) Hellwinkel, D. *Top. Curr. Chem.* **1983**, *109*, 1–63.

(12) (a) Kojima, S.; Kajiyama, K.; Akiba, K.-y. *Tetrahedron Lett.* **1994**, *35*, 7037–7040. (b) Akiba, K.-y.; Matsukawa, S.; Kajiyama, K.; Nakamoto, M.; Kojima, S.; Yamamoto, Y. *Heteroat. Chem.* **2002**, *13*, 390–396. (c) Kojima, S.; Kajiyama, K.; Nakamoto, M.; Matsukawa, S.; Akiba, K.-y. *Eur. J. Org. Chem.* **2006**, 218–234. (d) Kajiyama, K.; Yoshimune, M.; Kojima, S.; Akiba, K.-y. *Eur. J. Org. Chem.* **2006**, 2739–2746. (e) Kojima, S.; Nakamoto, M.; Akiba, K.-y. *Eur. J. Org. Chem.* **2008**, 1715–1722.

(13) (a) Oda, R.; Huc, I.; Schmutz, M.; Candau, S. J.; MacKintosh, F. C. *Nature* **1999**, *399*, 566–569. (b) Lacour, J.; Hebbe-Viton, V. *Chem. Soc. Rev.* **2003**, *32*, 373–382. (c) Hamilton, G. L.; Kang, E. J.; Mba, M.; Toste, F. D. *Science* **2007**, *317*, 496–499.

(14) (a) Wasserscheid, P., Welton, T., Eds. *Ionic Liquids in Synthesis*; Wiley-VCH: Weinheim, Germany, 2003. (b) Rogers, R. D.; Seddon, K. R. *Science* **2003**, *302*, 792–793. (c) Schulz, P. S.; Müller, N.; Bösmann, A.; Wasserscheid, P. *Angew. Chem., Int. Ed.* **2007**, *46*, 1293–1295. (d) Bica, K.; Gaertner, P. *Eur. J. Org. Chem.* **2008**, 3235–3250.

(15) (a) Windus, T. L.; Gordon, M. S.; Davis, L. P.; Burggraf, L. W. *J. Am. Chem. Soc.* **1994**, *116*, 3568–3579, and references therein. (b) Yanai, T.; Taketsugu, T.; Hirao, K. *J. Chem. Phys.* **1997**, *107*, 1137–1146. (c) Deiters, J. A.; Holmes, R. R. *Organometallics* **1996**, *15*, 3944–3956.

(16) Frisch, M. J.; et al. *Gaussian 03*, Revision B.05; Gaussian, Inc.: Wallingford CT, 2004.

(17) Krossing, I.; Raabe, I. *Angew. Chem., Int. Ed.* **2004**, *43*, 2066–2090.

(18) Sullivan, S. A.; DePuy, C. H.; Damrauer, R. *J. Am. Chem. Soc.* **1981**, *103*, 480–481.

(19) (a) Adams, D. J.; Clark, J. H.; Hansen, L. B.; Sanders, V. C.; Tavener, S. J. *J. Fluorine Chem.* **1998**, *92*, 123–125. (b) Maggiarosa, N.; Tyrra, W.; Naumann, D.; Kirij, N. V.; Yagupolskii, Y. L. *Angew. Chem., Int. Ed.* **1999**, *38*, 2252–2253. (c) Soli, E. D.; Manoso, A. S.; Patterson, M. C.; DeShong, P. *J. Org. Chem.* **1999**, *64*, 3171–3177.

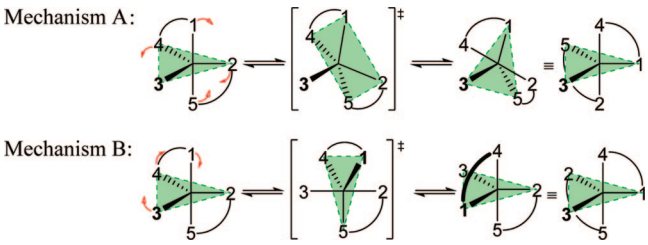

Figure 1. Ligand permutation mechanisms for bis(biaryl)silicates.

in the order ap < eq < bas < ax,[5,20] and this difference in chemical nature of the bonding sites is important when we consider the arrangement of substituents and the substituent effects.

The crystal structures of spirocyclic bis(biaryl)silicates[3,4] show an approximate TBP geometry with a distortion to RP along the Berry pathway[21] of only 7% for **1b**, 7%/9% for **1c** (two independent molecules), and 16% for **2b**. In each case, the monodentate substituent occupies an eq site and each biaryl group bridges one axial and one equatorial site (ax,eq) (Figure 1) to afford a propeller-like shape. Two stereomutations can be discerned with each leading to inversion of the helicity. Mechanism A corresponds to the Berry pseudorotation,[8,9] that is, the two ax aryl subunits (1, 5) bend toward each other as two eq aryl subunits (4, 2) bend away. This route proceeds through an RP-type transition state (TS) with the biaryl moieties in bis-basal positions and the monodentate substituent in the apical position. Mechanism B corresponds to Muetterties' process 4[9] and involves the cyclic permutation of the monodentate group (3) with the eq (4) and ax (1) Si−C bonds of one biaryl group (Figure 1). The TBP-type TS has the monodentate group in an axial position and one biaryl moiety bis-equatorial. Previously, we have shown that this geometry is over 10 kcal mol^{-1} higher in energy than that with both biaryl groups in ax,eq positions, which is due to the repulsive overlap between the aromatic π-system of the eq,eq biaryl moiety and the Si−C axial bonds.[5]

Next, we discuss the geometric and energetic aspects for each route in detail at the B3LYP/L//B3LYP/S (L = 6-311++G(2d,p), S = 6-31G(d)) level[16] for pentaorganosilicate **1**, which will serve as reference for the silicates **2**, **5**, and **6**.

Racemization of 1 via Mechanism A. For this process one might expect a C_s symmetric TS in which the interchanging biphenyl groups are symmetry-equivalent, i.e. [**1RP**] (Figure 2). However, in this geometry there is considerable steric repulsion between the four biphenyl hydrogen atoms ortho to silicon with H···H contacts of only 1.837 and 1.840 Å (cf., the van der Waals contact distance is 2.40 Å). Also, each biphenyl moiety is rather bent and concave when viewed from the ap Me group with a 21.9° angle between the planes of the phenyl subunits. As a result, [**1RP**] is 17.6 kcal mol^{-1} higher in energy than **1** and constitutes a second-order saddle point, associated with the desired Berry-type motion (84 cm^{-1}) and with bending of either one of the biphenyl groups to become convex (35 cm^{-1}).

Instead, mechanism A bifurcates into two enantiomeric reaction paths[22] that differ only as to which of the biphenyl groups becomes concave and which one becomes convex. The associated potential energy surface is depicted in Figure 2. During the first part of the process, the energy rises steeply as two *o*-H atoms have to pass each other with a minimum H···H distance of 1.682 Å ([**1H**]). Then, the energy profile flattens out quickly as the biphenyl groups slide one underneath the other, reaching the TS [**1A**]‡ at 15.5 kcal mol^{-1}. Its RP-type geometry is still rather strained, featuring two H···H contacts of 2.025 Å, while one of the biphenyl moieties is 27.7° concave, and the other, 17.7° convex.

Racemization of 1 via Mechanism B. Figure 3 shows the reaction profile for the interconversion of Λ-**1** to Δ-**1** via TS [**1B**]‡, which has a TBP-type geometry with the methyl group in an axial position. This transition structure is 10.2 kcal mol^{-1} higher in energy than **1**, which is mainly due to repulsion between the eq,eq biphenyl π-system and the electron-rich axial Si−C bonds.[5] Along the reaction coordinate, we identified the nonstationary geometry [**1S**] and its mirror image [**1S′**] that have skewed RP arrangements with the apex at 78° above the center of the basis; the methyl group is in a basal position. In these structures, π-repulsion is already present between the ap,bas biphenyl group and the adjacent basal Si−Me and Si−C_{Ar} bonds. The reaction coordinate for pathway B thus reflects two consecutive Berry-type deformations; note that the connecting TBP-type [**1B**]‡ is a transition structure.

The reaction barrier for mechanism B is a significant 5 kcal mol^{-1} lower in energy than that for mechanism A because of the much less severe steric interactions. The only interatomic repulsion in [**1B**]‡ is that between the ax methyl group and the nearby *o*-H atom of the ax,eq biphenyl moiety with a C···H distance of 2.503 Å (cf. 2.90 Å van der Waals sum).

Validation of Computational Method. In a recent benchmark study, Bento et al.[23] showed B3LYP/TZ2P to perform well for nucleophilic substitution at carbon and silicon. The key factors that govern the barrier heights for ligand permutation (i.e., *o*-H repulsion and π-interaction) cannot be investigated with model systems small enough for such high-level benchmarking, but an even better performance is expected because the coordination number of silicon does not change.

We validated B3LYP/L//B3LYP/S (L = 6-311++G(2d,p), S = 6-31G(d)) for the experimentally determined stereomutational barrier of the well-characterized silicate **1** (Table 1).[2,3] Optimization at the B3LYP/L level afforded virtually identical geometries and reaction barriers. The stabilization by the solvent THF, probed by subsequent single-point calculations with the polarizable continuum model (PCM),[24] is very similar for all structures, ranging from −22.9 for [**1B**]‡ to −24.1 kcal mol^{-1} for [**1RP**]‡ and thus has a negligible influence on the relative energies. Electron correlation (MP2/S) resulted in shortening

(20) Hoffmann, R.; Howell, J. M.; Muetterties, E. L. *J. Am. Chem. Soc.* **1972**, *94*, 3047–3058.
(21) Based on the dihedral angle sum method:(a) Holmes, R. R.; Day, R. O.; Harland, J. J.; Sau, A. C.; Holmes, J. M. *Organometallics* **1984**, *3*, 341–347. (b) Holmes, R. R.; Deiters, J. A. *J. Am. Chem. Soc.* **1977**, *99*, 3318–3326.
(22) (a) Wolfe, S.; Schlegel, H. B.; Csizmadia, I. G.; Bernardi, F. *J. Am. Chem. Soc.* **1975**, *97*, 2020–2024. (b) Bifurcation of the stereomutation path has been reported earlier for SiH_4F^- and PH_4F, see refs 15a and b. In these cases, four equivalent minima are connected by a single TS (i.e. a branching of the reaction path toward the reactants and the products) as opposed to the interchange of Λ- and Δ-**1** via two equivalent TSs [**1A**]‡.
(23) Bento, A. P.; Solà, M.; Bickelhaupt, F. M. *J. Comput. Chem.* **2005**, *26*, 1497–1504.
(24) (a) Grimme, S. *J. Chem. Phys.* **2003**, *118*, 9095–9102. (b) Goumans, T. P. M.; Ehlers, A. W.; Lammertsma, K.; Würthwein, E.-U.; Grimme, S. *Chem. Eur. J.* **2004**, *10*, 6468–6475.
(25) Cossi, M.; Scalmani, G.; Rega, N.; Barone, V. *J. Chem. Phys.* **2002**, *117*, 43–54.

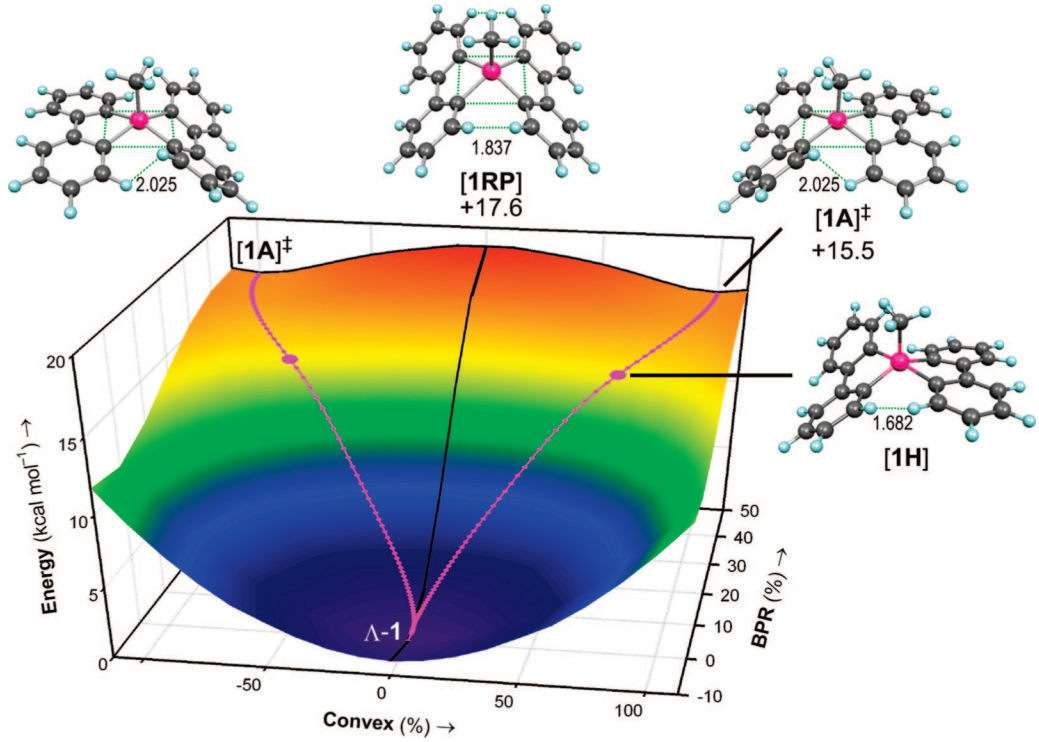

Figure 2. Potential energy surface for stereomutation of Λ-**1** to Δ-**1** via mechanism A, with projected enantiomeric IRC pathways in pink and Berry pseudorotation (BPR) and convex/concave pathways in black. H···H contact distances are given in Å.

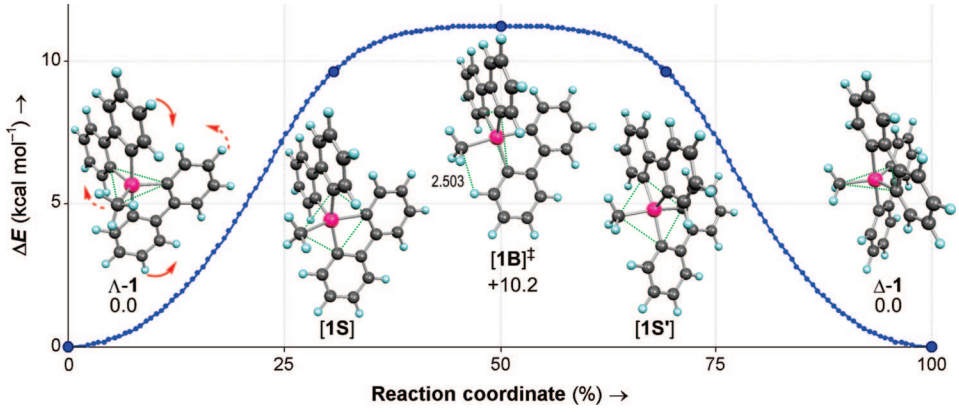

Figure 3. Pathway B for racemization of **1** via a TBP geometry with axial methyl group.

Table 1. Evaluation of Solvation and Electron Correlation Effects on the Calculated Stereomutation Barriers of **1** (ΔE in kcal mol^{-1})

method[a]	[1A]‡	[1B]‡	[1RP]
B3LYP/L//B3LYP/S	15.5	10.2	17.6
B3LYP/L	15.5	10.2	17.5
B3LYP/L/PCM(THF)//B3LYP/L	15.2	10.7	16.8
SCS-MP2/L//MP2/S	15.5	9.3	18.2

[a] L = 6-311++G(2d,p), S = 6-31G(d).

Table 2. B3LYP/L//B3LYP/S and Experimental[2] Gibbs Free Energy Barriers (kcal mol^{-1}) for Substituent Permutation in **1**

	$\Delta G^{\ddagger}_{298K}$	$\Delta G^{\ddagger}_{247K}$
mechanism A	16.5	16.3
mechanism B	11.4	11.1
exp. barrier		13

of the polar covalent Si−C bonds by only 0.01 (eq,ap) to 0.02 Å (ax,bas), while the reaction barriers are hardly affected at the SCS-MP2/L//MP2/S level.[25]

Finally, we compared the B3LYP/L//B3LYP/S and experimentally determined[2] Gibbs activation energies for ligand permutation in **1** (Table 2). The calculated $\Delta G^{\ddagger}_{247_K}$ of 11.1 kcal mol^{-1} for racemization via mechanism B is significantly lower than that for mechanism A (16.3 kcal mol^{-1}). We consider this ordering to be reliable because only conformational changes are involved, which leads to the conclusion that ligand interchange in **1** takes place preferentially via route B. The calculated barrier is in good agreement with the experimental value of 13 kcal mol^{-1}.

Since B3LYP/L//B3LYP/S performs very satisfactorily for **1** and enables the treatment of larger molecules without excessive computational cost, we will use this method likewise for the other silicates.

Bis(biphenyl)fluorosilicate 5. We synthesized fluorosilicate **5** to study the influence of the monodentate substituent (Me (**1**) vs F (**5**)). Treatment of bis(biphenyl-1,1′-diyl)silane (**7**) with 2

Scheme 1. Synthetic Route to Fluorosilicates **5**

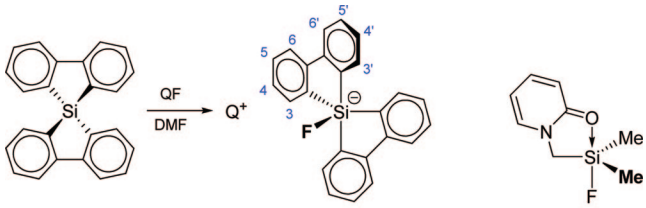

7 **5a**: $Q^+ = Cs^+$ **b**: $Q^+ = Me_4N^+$ **8**

equiv of anhydrous CsF or meticulously dried TMAF[26] in DMF resulted in the near-quantitative formation of silicates **5a** and **5b**, respectively (Scheme 1). Both compounds were fully characterized in solution[27] by NMR spectroscopy and showed virtually identical spectra. The ^{29}Si resonance of **5a** is shifted strongly upfield from −6.4 (**7**) to −90.6 ppm, which is characteristic of pentacoordination, but is less shielded than in **1** ($\delta_{Si} = -105.5$ ppm)[2] due to the more electron-withdrawing nature of the fluorine substituent. The single-bond Si−F coupling of 291.2 Hz is fairly large (cf. $SiPh_3F_2^-$: 252,[28] $SiMe_3(CF_3)F^-$: 235 Hz[19b]), which we attribute to eq placement of the pendant fluorine (see below).[5] The fluorine nucleus is deshielded at $\delta_F = -116.4$ ppm (cf. TMAF in DMF: −82.9 ppm) in accordance with its mixed covalent−ionic bonding.[5] For comparison, **8** ($\delta_F = -116.7$ ppm) features 30% O→Si and 70% Si−F bond formation, as elegantly shown by Bassindale et al.[29]

Variable-temperature NMR showed that **5b** is stable up to at least 87 °C and that it is the sole species even when cooled down to −55 °C. Throughout this temperature range, the ^{1}H and ^{13}C aromatic regions featured only four and six sharp resonances, respectively, implying that all phenyl subunits are NMR equivalent. A C_{2v} symmetric structure [**5RP**] (Figure 4) would suffer from severe *o*-H repulsion analogous to [**1RP**], and would have the highly electronegative fluorine in the least favorable, apical position.[20,5] Hence, the NMR equivalence of the phenyl moieties must be the result of rapid intramolecular substituent interchange as Si−F or Si−C bond dissociation−association can be ruled out on the basis of the persistent $^1J_{SiF}$ coupling and the high-quality ^{1}H,^{29}Si ge-HMBC NMR spectrum of **5b**, which shows not only a strong correlation of silicon with H3/H3′ but even the weaker correlations with H4/H4′ and H6/H6′.

The B3LYP/L//B3LYP/S calculations confirm that the global minimum of **5** has a TBP-type coordination with the fluorine in an eq position (Figure 4), while [**5RP**] is a second-order saddle point, 25.0 kcal mol^{-1} less stable than **5**. The calculated barrier for Berry pseudorotation via mechanism A is rather high (22.6 kcal mol^{-1}). As the RP-like TS [**5A**]‡ is similar in geometry to [**1A**]‡, the 7.1 kcal mol^{-1} higher barrier for [**5A**]‡ expresses the unfavorable effect of apical placement of a strongly electronegative substituent.[5] In contrast, ligand interchange via mechanism B has a barrier as low as 2.3 kcal mol^{-1} ([**5B**]‡) due to the strong preference of fluorine to occupy an electron-rich axial site, which opposes the π-repulsion from the eq,eq placed biphenyl group. Thus, the very rapid epimerization of **5** via route B renders all phenyl moieties equivalent on the NMR time scale. In general, the opposing effect of the electronegativity of the monodentate substituent on the barrier heights of mechanism A vs B allows control over the preferred stereomutational pathway.

Chart 2. Configurational Isomers of **2**

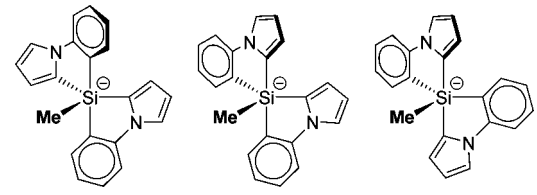

Λ-**2I** Λ-**2II** Λ-**2III**

Configurational Isomerization of 2. We now turn our attention to the biaryl ligands. As compared to the biphenyl groups in **1**, the phenylpyrrole moieties in **2** have a higher π-electron density and a slightly smaller steric demand. Each phenylpyrrole ligand can adopt two ax,eq orientations, i.e. with either the phenyl or the pyrrole moiety at the axial site. As a result, there are six conformational isomers of **2** that have both bidentate groups in an ax,eq arrangement, namely the three enantiomeric pairs Λ/Δ-**2I**-**III** (Chart 2). **2I** was calculated to be the most stable one, in accord with the reported X-ray crystal structure for **2b**,[4] while also **II** and **III** are both local minima at $\Delta E = 1.7$ and 2.4 kcal mol^{-1}, respectively. We attribute the equatorial site preference of the pyrrole moiety to its higher π-electron density as compared to the phenyl moiety, causing some extra repulsive overlap of the ax pyrrole π-orbitals with the eq Si−C bonds in **II** and **III**.[5]

The isomers of **2** can interconvert according to the exchange graph shown in Figure 5.[30] Conformers **I** and **III** can interchange directly via mechanism A (vertical reaction arrows). Similar to **1**, bifurcation of the reaction pathway occurs with the degenerate TSs [**2A**]‡ having an RP-like geometry with one concave and one convex bas,bas biaryl group. We use the indices δ and λ to indicate that the degenerate TSs (δ) between Λ-**2I** and Δ-**2III** are the mirror images of those (λ) between Δ-**2I** and Λ-**2III**.[31] Racemization of isomer **2II** also proceeds by means of mechanism A, i.e., via the degenerate RP-like TSs [λ/δ-**2A′**]‡. The corresponding C_s symmetric RP geometry with two concave biaryl groups ($\Delta E = 12.6$ kcal mol^{-1}, structure not shown) is, as expected, a second-order saddle point. The barriers of 10.5 ([**2A**]‡) and 12.1 kcal mol^{-1} ([**2A′**]‡) are notably lower than that of 15.5 kcal mol^{-1} for [**1A**]‡ (see Table 1), since the *o*-H atoms of the smaller five-membered pyrrole rings in the RP-like TSs

(26) Christe, K. O.; Wilson, W. W.; Wilson, R. D.; Bau, R.; Feng, J. *J. Am. Chem. Soc.* **1990**, *112*, 7619–7625.

(27) After several attempts to recrystallize **5a** from DMF, colorless blocks were obtained that were shown by X-ray analysis to be 1,1,5,5-tetrakis(biphen-2-yl)-3,3,7,7-tetramethyltetrasiloxane (see Supporting Information). This compound is likely formed by reaction with silicone grease and adventitious water and stresses the high reactivity of the fluorosilicate. Cooling a solution in grease-free glassware in the freezer of a glovebox repeatedly afforded an amorphous solid.

(28) (a) Pilcher, A. S.; Ammon, H. L.; DeShong, P. *J. Am. Chem. Soc.* **1995**, *117*, 5166–5167. (b) Handy, C. J.; Lam, Y.-F.; DeShong, P. *J. Org. Chem.* **2000**, *65*, 3542–3543.

(29) Bassindale, A. R.; Baukov, Y. I.; Borbaruah, M.; Glynn, S. J.; Negrebetsky, V. V.; Parker, D. J.; Taylor, P. G.; Turtle, R. *J. Organomet. Chem.* **2003**, *669*, 154–163.

(30) Such graphs have been derived for related cases, and are simplifications of the general Desargues−Levi graph for pentacoordinate stereomutations; see refs 9b,11a,12c,e and:(a) Lauterbur, P. C.; Ramirez, F. *J. Am. Chem. Soc.* **1968**, *90*, 6722–6726. (b) Mislow, K. *Acc. Chem. Res.* **1970**, *3*, 321–331.

(31) When viewing each TS from the Me group, the foremost phenylpyrrole bidentate ligand ([**2A**]‡, [**2A′**]‡: concave group; [**2B**]‡, [**2B′**]‡: eq,eq group) has its phenyl ring either in a clockwise (δ) or an anticlockwise (λ) direction with respect to its pyrrole ring.

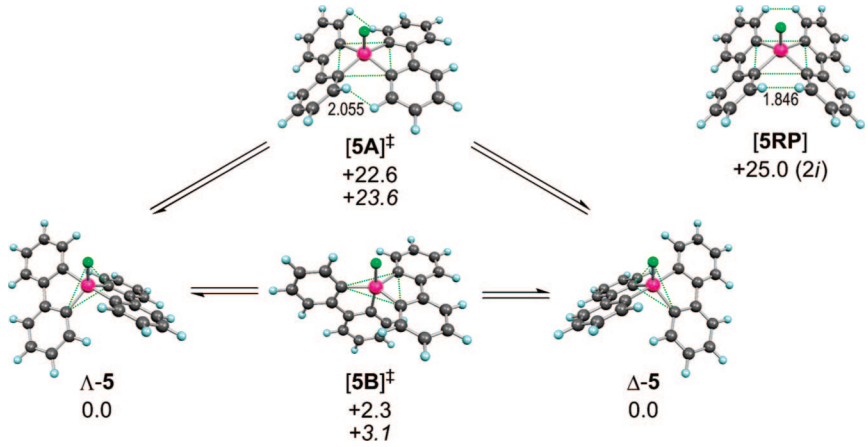

Figure 4. Exchange graph[30] for **5**, with B3LYP/L//B3LYP/S relative energies (kcal mol^{-1}) and Gibbs free energies ΔG_{298K} in italics.

of **2** protrude less toward the other bidentate ligand. As a result, the bas,bas biaryl groups are less distorted from planarity ([**2A**]‡: 19.3°/8.7°, [**2A′**]‡: 19.1°/8.5° concave/convex) than in [**1A**]‡.

Alternatively, ligand permutation via mechanism B (horizontal reaction arrows) leads to interchange between **I** and **II**, and between **II** and **III**. Again, the respective TSs [**2B**]‡ and [**2B′**]‡ have a TBP-like geometry with the methyl substituent in an axial position. In [**2B**]‡ the second ax site is occupied by a pyrrole moiety versus a phenyl moiety in [**2B′**]‡. We use the same λ/δ convention as for [**2A**]‡ to indicate the mirror images of each TS.[31] As the phenylpyrrole moiety is more π-electron rich than a biphenyl group, both TSs suffer from increased π-repulsion of the eq,eq biaryl group with the ax bonds. As a result, the barriers for route B are raised from 10.2 kcal mol^{-1} for [**1B**]‡ to 16.3 for [**2B**]‡ and to 13.1 kcal mol^{-1} for [**2B′**]‡. Therefore, exchange mechanism A is favored over mechanism B for **2** in contrast to silicates **1** and **5**.

Comparison with Experiment for 2. Earlier we studied the thermodynamics and kinetics of the **2I** ↔ **2II** equilibrium by variable-temperature NMR.[4] The calculated higher Gibbs free energy of 1.7 kcal mol^{-1} for **2II** (Table 3) is in excellent agreement with the experimental $\Delta_r G_{258K} = 1.66(6)$ kcal mol^{-1}, while that for **2III** is still higher (2.4 kcal mol^{-1}). The calculations show that direct **2I** ↔ **2II** interchange (via [**2B**]‡, $\Delta G^{\ddagger}_{258K} = 17.1$ kcal mol^{-1}) is less favorable than isomerization via **2III**, of which the rate-limiting step has a barrier of 13.9 kcal mol^{-1} ([**2B′**]‡), which agrees very well with the experimental reaction barrier of 15.5(5) kcal mol^{-1}.[32] Although pseudorotamer **2III** should thus be readily accessible, its concentration is likely too low for detection by NMR; the relative Boltzmann population of **2III** at 258 K is estimated at only 0.9% (**2I**: 92.6%, **2II**: 6.5%). Moreover, its NMR signals would coalesce with those of the main isomer due to the rapid **2I** ↔ **2III** equilibrium ($\Delta G^{\ddagger}_{258K} = 11.3$ kcal mol^{-1}, [**2A**]‡) so that lower temperatures would be required to freeze this process on the NMR time scale, but this would also cause an even lower population of **2III**.

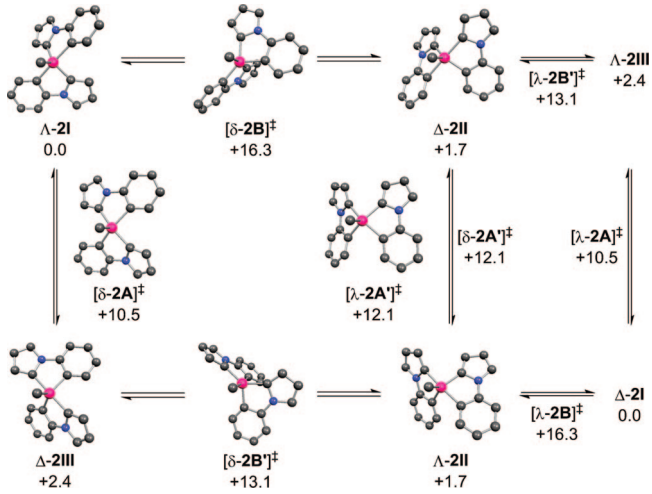

Figure 5. Exchange graph for **2**, with B3LYP/L//B3LYP/S relative energies in kcal mol^{-1}. Indices Λ and Δ (λ and δ)[31] denote the mirror images of each minimum (TS). Hydrogen atoms are omitted for clarity.

Table 3. B3LYP/L//B3LYP/S and Experimental[4] Gibbs Free Energies (kcal mol^{-1}) for Configurational Isomerism of **2I**

conformer	ΔG_{298K}	ΔG_{258K}	TS	$\Delta G^{\ddagger}_{298K}$	$\Delta G^{\ddagger}_{258K}$
2II	1.7	1.7	**2A**	11.5	11.3
2III	2.4	2.4	**2A′**	13.0	12.9
			2B	17.4	17.1
			2B′	14.2	13.9
exp. isomer		1.66(6)	exp. barrier		15.5(5)

Design of a Configurationally Rigid Silicate. The preceding analyses of **1**, **2**, and **5** reveal how the stereomutations can be slowed down. That is, electronegative monodentate substituents disfavor process A, while path B is inhibited by π-electron-rich biaryl bidentate groups. Substitution of the biaryl groups ortho to silicon impedes process A, but the size of the substituents requires tuning to avoid steric crowding in the silicate's TBP-like ground state, which reduces its stability.[5,33] By manipulating these features it should be possible to design configurationally rigid, Si-chiral pentaorganosilicates.

We decided to enlarge the phenyl moieties in **2** to rigid naphthyls as in pentaorganosilicate **6**, which should strongly hinder ligand permutation via route A. These larger naphthyl moieties should hardly affect the stability of conformer Λ/Δ-**6I** (Chart 3), since each occupies a less crowded axial site,

(32) The experimentally determined barrier does not indicate which stereomutational route is preferred, because both calculated barriers deviate equally as much, albeit in opposite directions. However, the calculated ordering of the barriers is more reliable because both TSs relate to stereomutations via mechanism B. We note that also for **1** the calculated barrier is slightly lower than that measured in solution, to a comparable extent as for [**2B′**]‡

(33) (a) Bento, A. P.; Bickelhaupt, F. M. *J. Org. Chem.* **2007**, *72*, 2201–2207. (b) Pierrefixe, S. C. A. H.; Fonseca Guerra, C.; Bickelhaupt, F. M. *Chem. Eur. J.* **2008**, *14*, 819–828.

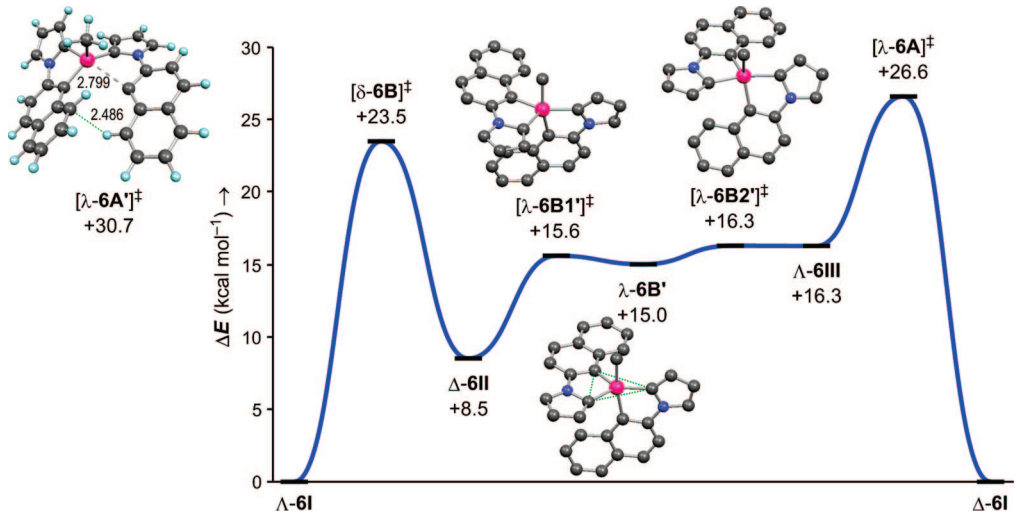

Figure 6. B3LYP/L//B3LYP/S energy profile for racemization of **6I**, with selected geometries; hydrogen atoms are omitted for clarity. Indices Λ and Δ (*λ* and *δ*) denote the stereochemistry of each stationary point.[31] On the left TS [*λ*-**6A′**]‡ for deformation of Δ-**6II** via pathway A (not shown).

Table 4. B3LYP/L//B3LYP/S Gibbs Free Energies (kcal mol^{-1}) for Configurational Isomerism of **6I**

conformer	ΔG_{298K}	TS	$\Delta G^{\ddagger}_{298K}$
6II	8.6	**6A**	27.4
6III	15.0	**6A′**	30.9
6B′	14.6	**6B**	24.0
		6B1′	16.2
		6B2′	16.9

Table 5. BP86/TZP Si−Me Bonding Energy Analyses (kcal mol^{-1})

	1	**2I**	**6I**
ΔE_{Pauli}	266.3	272.2	279.5
ΔV_{elstat}	−213.7	−218.6	−221.0
ΔE_{oi}	−163.7	−169.8	−177.9
ΔE_{int}	−111.1	−116.1	−119.5
ΔE_{prep}	49.1	46.5	49.3
ΔE_{net}	−62.0	−69.6	−70.2

staggered with respect to the eq methyl and the pyrrole moiety of the other biaryl group. In contrast, configurations **6II** and **6III** suffer from considerable steric congestion between the eq naphthyl and the nearby ax group(s). Ligand interchange via route B is likewise impeded because of the *π*-electron-rich pyrrole moieties, which is complemented in TBP-like TS [**6B**]‡ by steric interactions between the eq naphthyl moiety and the ax methyl group.

Configurational Isomerism of Bis(naphthylpyrrole)silicate 6. The expectations were confirmed by B3LYP/L//B3LYP/S calculations that show **6II** and **III** to be respectively 8.5 and 16.3 kcal mol^{-1} less stable than **I** (Figure 6), which is a much larger energy difference than for the corresponding isomers of **2** (i.e., ΔE = 1.7 and 2.4 kcal mol^{-1}).[4] Steric congestion is indeed the origin of the destabilization and this is reflected in the short distances between the eq H8′ and ax C_{ipso} atoms (**6II**: 2.291; **6III**: 2.303(3) Å) and in the lengthening of the eq Si−Naph bonds (e.g., **6II**: 1.989 vs 1.906 Å for the eq Si−Pyr bond). The calculations also show that enantiomerization via pathway A is prohibited for **6II**. In TS [**6A′**]‡ (ΔE = 30.7 kcal mol^{-1}; cf. [**2A′**]‡: 12.1 kcal mol^{-1}) the Naph moieties have a close C···H contact of 2.486 Å (Figure 6 left) with a continued motion leading to Si−C_{Naph} bond dissociation.

Chart 3. Configurational Isomers of **6**

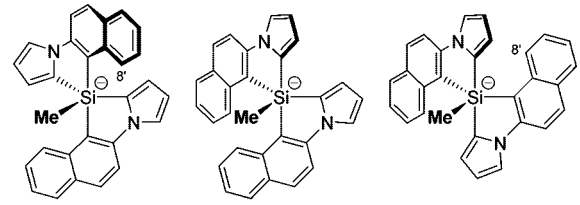

Λ-**6I** Λ-**6II** Λ-**6III**

Hence, racemization of **6I** can only take place via TS [**6A**]‡, that is, via **6II** and **6III** (cf. exchange graph for **2**, Figure 5), for which the calculated energy profile is shown in Figure 6. As anticipated, the high barriers for [**6A**]‡ and [**6B**]‡ of $\Delta G^{\ddagger}_{298K}$ = 27.4 and 24.0 kcal mol^{-1}, respectively (Table 4) effectively prevent configurational isomerization at room temperature. Interestingly, the calculational survey also identifies the TBP-like structure **6B′** as a shallow minimum for the interconvertion of **6II** and **6III**. As a result, pathway B represents two Berry pseudorotations with TSs [**6B1′**]‡ and [**6B2′**]‡, which have skewed RP-like geometries (cf. [**1S**]). Although the conversion of [**6B2′**]‡ to **6III** involves a significant change in geometry (i.e., from 73% to 30% RP), there is little influence on the relative energy because the reduction in *π*-repulsion is offset by the increase in steric crowding by the Naph moieties.

Viability of Silicate 6I. Having established that **6I** is unlikely to undergo Si-epimerization, we next address its intrinsic stability, as we showed before[5] that steric congestion facilitates decomposition by heterolytic bond cleavage. To this end, we performed Si−Me bonding energy analyses[5] of silicates **1**, **2I**, and **6I** with ADF[34,35] at BP86/TZP (Table 5). The preparation energy ΔE_{prep} is governed by the deformation of the silane

(34) (a) te Velde, G.; Bickelhaupt, F. M.; van Gisbergen, S. J. A.; Fonseca Guerra, C.; Baerends, E. J.; Snijders, J. G.; Ziegler, T. *J. Comput. Chem.* **2001**, *22*, 931–967. (b) Fonseca Guerra, C.; Snijders, J. G.; te Velde, G.; Baerends, E. J. *Theor. Chem. Acc.* **1998**, *99*, 391–403. (c) *ADF2004.01, SCM, Theroretical Chemistry*; Vrije Universiteit: Amsterdam, The Netherlands; http://www.scm.com.

(35) (a) Morokuma, K. *Acc. Chem. Res.* **1977**, *10*, 294–300. (b) Ziegler, T.; Rauk, A. *Inorg. Chem.* **1979**, *18*, 1755–1759. (c) Ziegler, T.; Rauk, A. *Theor. Chim. Acta* **1977**, *46*, 1–10. (d) Bickelhaupt, F. M.; Baerends, E. J. In *Reviews in Computational Chemistry*; Lipkowitz, K. B., Boyd, D. B., Eds.; Wiley: New York, 2000; Vol. 15, pp 1−86.

Scheme 2. Synthetic Route for Silicate **6**, with Numbering Scheme for the Bidentate Ligand

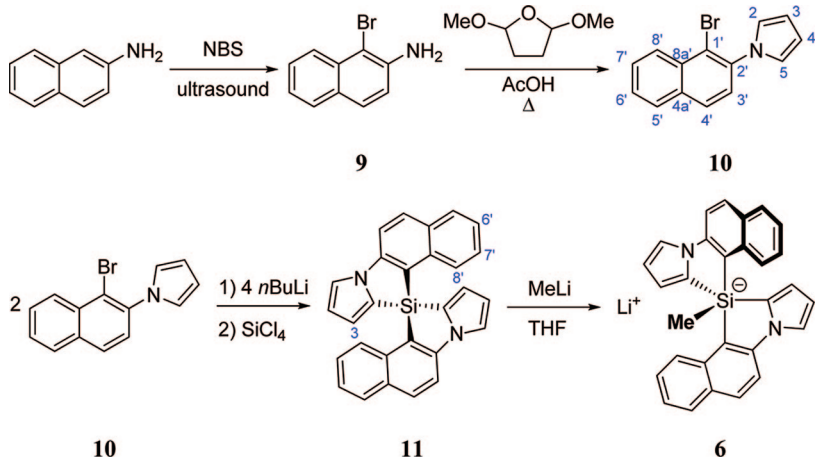

fragment and is indicative for the steric congestion between the biaryl groups. Silicates **1** and **6I** have similar ΔE_{prep} of 49.1 and 49.3 kcal mol^{-1}, respectively, while that for **2I** is slightly smaller (46.5 kcal mol^{-1}). The trend in Pauli repulsion ΔE_{Pauli} between the silane and methyl anion fragments is countered by the orbital interaction term ΔE_{oi}, indicating that the fragment orbital overlap increases in the order **1** < **2I** < **6I** (Table 5). The electrostatic attraction ΔV_{elstat} increases along the same series (**1**: −213.7, **2I**: −218.6, **6I**: −221.0 kcal mol^{-1}) due to charge withdrawal from silicon. This leads to the conclusion that **6I** should be stable against heterolytic Si−Me bond dissociation, like **2I**, while it experiences no significant extra steric congestion. The (axial) Si−C_{Biaryl} bonds cannot be analyzed readily, because bond scission does not afford two separate fragments. However, the calculated high relative energy of the TS [**6A′**]‡ (see Table 4) suggests that **6I** is also sufficiently stable against such heterolytic cleavage. Therefore, we set out to generate silicate **6** experimentally.

Synthesis of Bis(naphthylpyrrole)silicate 6. Our synthetic approach to **6** (Scheme 2) is similar to that reported earlier for **2**.[4] Commercial β-naphthylamine was brominated selectively at C1,[36] and subsequent condensation with 2,5-dimethoxytetrahydrofuran afforded bromonaphthylpyrrole **10** (98%).[37] The desired spirocyclic silane **11** was obtained in 85% yield from **10** by treatment with *n*-butyllithium and $SiCl_4$.[37] Silane **11** exhibits a characteristic ^{29}Si NMR chemical shift of $\delta = -36$ ppm (cf. phenylpyrrole analogue: −35 ppm).[4] The naphthyl H8′ resonance of **11** at $\delta_H = 7.17$ ppm is shielded compared to that of **10** (8.39 ppm) and gives rise to an ABC pattern with H6′ and H7′.

Treatment of **11** with methyllithium in THF at −78 → 25 °C afforded a yellow solution of lithium silicate **6**, as evidenced by the upfield shift of the ^{29}Si NMR signal to $\delta = -129$ ppm (cf. **2**: −131 ppm). No change was observed for 2 days at room temperature, indicating the compound to be stable in solution.[38] Full NMR spectroscopic characterization of **6** suggests 2-fold symmetry, while the 2D NOESY spectrum showed correlations

Table 6. B3LYP/S Average H···H Distances (Å) for the Conformers of **6**

	H3···H8′	H3···Me	H8′···Me
6I	2.79	−[a]	2.27−2.73[b]
6II	5.47 eq−eq	3.13 ax	2.54 ax
6III	3.13	2.63−3.44[b]	−[a]

[a] Direct interaction not possible. [b] Assuming free methyl rotation.

of the naphthyl H8′ atoms with both the pyrrole H3 atoms and the methyl group. These observations are only compatible with geometry **6I**, in which the naphthyl H8′ atoms are situated in-between the eq methyl and pyrrole moieties; for comparison, Table 6 lists the calculated H···H distances for the three conformers of **6**. No NMR signals were observed that could be credited to traces of configurations **6II** or **III**.

Proof of Configurational Rigidity. To assess the stereorigidity of **6** as compared to **2**, we prepared the analogous ethyl silicates **12** and **13**, in which the ethyl CH_2 hydrogen atoms can serve as a diagnostic tool for epimerization at silicon. Namely, these CH_2 hydrogen atoms are diastereotopic and should show up as two separate double quartets in the ^{1}H NMR spectrum for a configurationally rigid silicate, whereas Si-epimerization would effectively cause interchange of the two resonances, leading to coalescence phenomena. On the other hand, the stereomutational barrier heights were expected to be hardly affected by substituting the methyl (**2**, **6**) for an ethyl group (**12**, **13**).

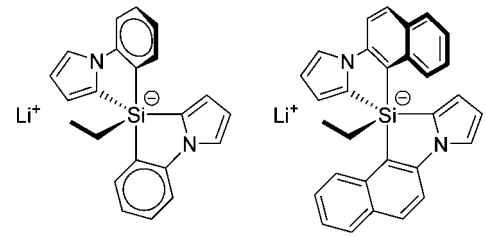

12 **13**

Indeed, at −50 °C silicate **12** featured two diastereotopic CH_2 hydrogen atoms that gave an AB_3C pattern with the terminal CH_3 group. The CH_2 signals broadened upon warming and coalesced at ∼50 °C, while the CH_3 signal evolved to a more regular triplet (see Supporting Information). These observations are consistent with Si-epimerization of **12** with an estimated barrier[39] of 16 kcal mol^{-1}, which parallels the 15.5 kcal mol^{-1} barrier reported previously for the analogous methylsilicate **2**.[4,40]

(36) Paul, V.; Sudalai, A.; Daniel, T.; Srinivasan, K. V. *Synth. Commun.* **1995**, *25*, 2401–2405.
(37) Analogous to ref 4 and. Cheeseman, G. W. H.; Greenberg, S. G. *J. Organomet. Chem.* **1979**, *166*, 139–152.
(38) Recrystallization of silicate **6** invariably afforded long, white needles that were too thin for X-ray structural analysis.
(39) Friebolin, H. *Basic One-and Two-Dimensional NMR Spectroscopy*, 3rd ed., Wiley-VCH: Weinheim, Germany, 1998; Chapter 11.

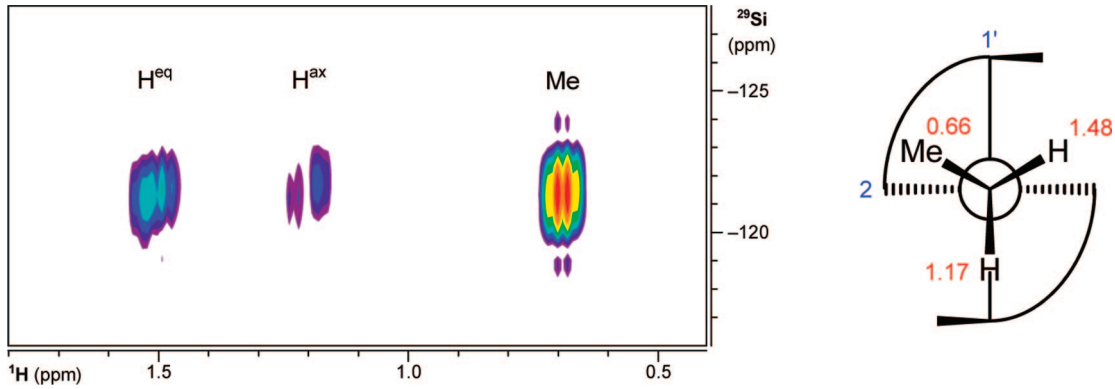

Figure 7. Left: ethyl region of the ^{1}H,^{29}Si ge-HBMC NMR spectrum of **13** at 300 K. Right: Newman projection along the Si-CH_2 bond with relevant hydrogen chemical shifts in red; for clarity, the naphthylpyrrole moieties are represented by arcs.

Also for silicate **13** separate CH_2 hydrogen signals were observed at δ_H = 1.17 and 1.48 ppm (Figure 7). Most importantly, the ^{1}H NMR spectra of **13** did not indicate any broadening or coalescence of the diastereotopic signals even at 55 °C. Moreover, a saturation transfer experiment at this temperature did not reveal any interchange within 5 s, which suggests a barrier of at least 21 kcal mol^{-1}. This unequivocally proves that **13** does not epimerize at silicon even beyond the NMR time scale, and indicates strongly that also methyl analogue **6** is indeed configurationally rigid.

Conclusions

Configurational isomerization of spirocyclic pentaorganosilicates occurs via two competitive routes (Figure 1). Route A bifurcates into two enantiomeric pathways with bent biaryl groups in the rectangular pyramidal transition structures. In route B the transition state has a trigonal bipyramidal structure with one biaryl group bridging two equatorial sites. DFT calculations at B3LYP/6-311++G(2d,p)//LYP/6-31G(d) reproduce the experimental kinetic and thermodynamic data. For spirocyclic **5**, the first synthesized tetraorganofluorosilicate, they show that substituent interchange via route B is strongly favored over that via route A in contrast to the methyl-substituted analogue **1**. Thus, the electronegativity of the monodentate substituent can be used to alter the preferred stereomutational route. The barrier of route A can also be increased by substitution of the biaryl groups ortho to silicon, while route B can be inhibited by using stronger π-donor bidentate systems and by ortho substitution. Accordingly, we designed and synthesized stable pentaorganosilicates, **6** and **13**, containing two naphthylpyrrole groups that are both sterically more demanding and more π-electron rich than biphenyls. Both the calculations and NMR spectroscopic data reveal that **6** and **13** are present in only a single conformation that does not epimerize at Si. Separation of the enantiomers Δ and Λ of these first configurationally rigid pentaorganosilicates is currently being pursued.

Computational Methods

General. All hybrid density-functional theory and second-order Møller−Plesset (MP2) theory calculations were carried out with Gaussian 03.[16] Geometries were optimized at the B3LYP/6-31G(d) level; the easy deformability of silicates required the use of an ultrafine integration grid and tight SCF and optimization convergence criteria. The nature of each stationary point was confirmed by a frequency calculation. The thermal corrections were scaled by the customary factor of 0.9804[41] and combined with single-point energies at the B3LYP/6-311++G(2d,p) level to afford the Gibbs free energies.

Validation. For **1**, successive geometry optimizations were performed at the B3LYP/6-311++G(2d,p) level, followed by B3LYP/6-311++G(2d,p) single-point energy calculations with the default polarizable continuum model (PCM),[24] specifying THF as the solvent. The cavity was built using the united atom topological model with radii optimized for the HF/6-31G(d) level (UAHF); the solute molecular symmetry was dismissed.

Additionally, geometries were optimized at the MP2/6-31G(d) level with tight SCF and convergence criteria. MP2/6-311++G(2d,p) single-point energies were then calculated, and the wave functions were tested for stability. The spin-component scaled SCS-MP2 energies[25] were obtained by combining the HF energies with the spin components $E_{\alpha\beta}$, scaled by 6/5, and $E_{\alpha\alpha}$ and $E_{\beta\beta}$, scaled by 1/3.

Reaction Profiles. Reaction profiles were obtained from IRC calculations at the B3LYP/6-31G(d) level, using a step size of 0.50 amu$^{1/2}$ Bohr. Details of the potential energy surface scan are provided in the Supporting Information.

Bonding Energy Analyses. Using the B3LYP/6-31G(d) geometries, silicate Si−Me bonds were analyzed in terms of fragment orbitals with the ADF 2004.01 package[34] at the BP86 level with an all-electron TZP basis set and an integration accuracy of 6.0.[5] The net bond energy ΔE_{net} is decomposed into four contributions:[35] the preparation energy ΔE_{prep} required for deformation of the fragments from their equilibrium structures to their geometries in the silicate; the Pauli repulsion (ΔE_{Pauli}) and electrostatic attraction (ΔV_{elstat}) between the fragments; and the orbital interaction energy ΔE_{oi} (negative, stabilizing):

$$\Delta E_{net} = E_{silicate} - (E_{silane} + E_{anion}) = \Delta E_{prep} + (\Delta E_{Pauli} + \Delta V_{elstat} + \Delta E_{oi}) \quad (1)$$

The latter three contributions are usually summed to give the interaction energy ΔE_{int}.

Experimental Section

General. Dimethylformamide (DMF) was distilled from phenylzinc iodide and stored on 3 Å molecular sieves, tetrachloromethane (CCl_4) from P_2O_5, diethyl ether (DEE) from lithium

(40) The ^{1}H,^{29}Si HMBC NMR spectrum at 223 K also suggested the presence of a second silicate at δ_{Si} = −121.2, correlating with a CH_3 resonance at δ_H = 0.80. We tentatively assign these signals to a minor configurational isomer, in line with our observations for **2**.

(41) (a) Foresman, J. B.; Frisch, A. *Exploring Chemistry with Electronic Structure Methods*, 2nd ed.; Gaussian Inc.: Pittsburgh, PA, 1996. (b) Wong, M. W. *Chem. Phys. Lett.* **1996**, *256*, 391–399.

(42) (a) Gilman, H.; Gorsich, R. D. *J. Am. Chem. Soc.* **1955**, *77*, 6380–6381. (b) Gilman, H.; Gorsich, R. D. *J. Am. Chem. Soc.* **1958**, *80*, 1883–1884.

aluminum hydride, and tetrahydrofuran (THF) from sodium/benzophenone. Commercial cesium fluoride (CsF) was dried in vacuo at >100 °C; tetramethylammonium fluoride (TMAF) was meticulously dried according to a literature procedure.[26] *N*-Bromosuccinimide (NBS) was recrystallized from boiling water and dried in vacuo over P_2O_5 in a desiccator; tetrachlorosilane was distilled before use to remove dissolved HCl gas. *n*-Butyllithium and methyllithium were purchased as 1.6 M solutions in hexanes and in diethyl ether, respectively; ethyllithium was purchased as a 0.5 M solution in benzene/cyclohexane (9:1). Bis(biphenyl-2,2′-diyl)silane (**7**) was synthesized from 1,1′-dibromobiphenyl and tetrachlorosilane analogous to ref 42; bis(phenylpyrrol-2,2′-diyl)-silane was synthesized according to ref 4. Silicates **5** were prepared and handled in the purified N_2 atmosphere of an MBRAUN Unilab glovebox; other syntheses were performed using standard Schlenk techniques. NMR spectra were recorded (at 298 K) on a Bruker Avance 250 (^{1}H, ^{13}C, ^{19}F) or a Bruker Avance 400 (^{1}H, ^{13}C, ^{29}Si, 2D spectra). NMR chemical shifts are internally referenced to the solvent for ^{1}H (DMF: 2.90, $CHCl_3$: 7.26, THF: 3.59 ppm) and ^{13}C (DMF: 35.19, $CDCl_3$: 77.16, THF: 67.58 ppm), and externally for ^{19}F to $CFCl_3$ and for ^{29}Si to TMS. Strongly coupled ^{1}H NMR signals were simulated to determine the chemical shifts and coupling constants. Melting points were measured on samples in sealed capillaries and are uncorrected. The high-resolution mass spectrum (HR-MS) of **5a** was measured on a JEOL JMS SX/SX 102A four-sector mass spectrometer, coupled to a JEOL MS-MP9021D/UPD system program. The sample was introduced via a direct insertion probe into the ion source (70 eV ionization potential), and heated to ∼300 °C. During the high-resolution EI-MS measurement a resolving power of 10,000 (10% valley definition) was used. The HR-MS of **5b** was measured on a Varian IonSpec FT-ICR mass spectrometer. A DMF solution of the sample was diluted into dry acetonitrile in the glovebox, and measured via electrospray ionization (ESI) in negative mode. Other HR EI-MS spectra were measured on a Finnigan Mat 900 mass spectrometer operating at an ionization potential of 70 eV.

Cesium Bis(biphenyl-2,2′-diyl)fluorosilicate (5a). CsF (71.45 mg, 470 μmol) and bis(biphenyl-2,2′-diyl)silane (73.95 mg, 222 μmol) were covered with DMF (3 mL), and the mixture was stirred for 2 days at room temperature. NMR revealed almost complete conversion to the silicate. The clear colorless supernate was filtered through glass wool and evaporated to afford crude **5a** as a white solid (101.60 mg, 94%). Mp: 221.5−226.1 °C; ^{1}H,^{29}Si ge-HMBC NMR (400.1 MHz, DMF): δ −90.6 (d, $^1J_{SiF}$ = 291.1 Hz); ^{19}F NMR (235.3 MHz, DMF): δ −116.4 ($^1J_{FSi}$ = 291.2 Hz); ^{13}C{^{1}H} NMR (100.6 MHz, DMF): δ 153.8 (d, $^2J_{CF}$ = 51.1 Hz, C2/2′), 146.2 (s, C1/1′), 134.4 (s, C3/3′), 126.4 (s, C5/5′), 124.8 (s, C4/4′), 118.5 (s, C6/6′); ^{1}H NMR (400.1 MHz, DMF): δ 7.71 (d, 4H, $^3J_{HH}$ = 7.6 Hz, H6/6′), 7.27 (d, 4H, $^3J_{HH}$ = 6.9 Hz, H3/3′), 7.09 (t, 4H, $^3J_{HH}$ = 7.4 Hz, H5/5′), 6.90 (t, 4H, $^3J_{HH}$ = 7.0 Hz, H4/4′); HR EI-MS: calcd for $C_{24}H_{17}FSi$ (M + H): 352.1084, found: 352.1093; *m/z*: 352 (27) $[M + H]^+$, 332 (100) $[M - F]^+$.

Tetramethylammonium Bis(biphenyl-2,2′-diyl)fluorosilicate (5b). Bis(biphenyl-2,2′-diyl)silane (35.9 mg, 108 μmol) and TMAF (21 mg, 225 μmol) were covered with DMF (1.0 mL). After thorough mixing, undissolved excess fluoride salt was precipitated by centrifugation, and the clear colorless supernate was transferred to a Schlenk. Evaporation of the solvent yielded crude **5b** as a white solid (47 mg, 99%). ^{29}Si{^{1}H} INEPT NMR (79.5 MHz, $^3J_{H,Si}$ = 4.5 Hz, 4H, DMF/C_6D_6): δ −91.2 (d, $^1J_{SiF}$ = 290.0 Hz); ^{19}F{^{1}H} NMR (235.3 MHz, DMF/C_6D_6): δ −116.8 ($^1J_{FSi}$ = 289.9, $^2J_{FC}$ = 51.3 Hz); ^{13}C{^{1}H} NMR (100.6 MHz, DMF/C_6D_6): δ 153.7 (d, $^2J_{CF}$ = 51.3 Hz, C2/2′), 146.2 (d, $^3J_{CF}$ = 3.4 Hz, C1/1′), 134.4 (d, $^3J_{CF}$ = 2.7 Hz, C3/3′), 126.4 (s, C5/5′), 124.9 (s, C4/4′), 118.5 (d, $^4J_{CF}$ = 1.9 Hz, C6/6′), 54.2 (t, $^1J_{C14N}$ = 3.8 Hz, Me_4N^+); ^{1}H NMR (400.1 MHz, DMF/C_6D_6): δ 7.75 (d, 4H, $^3J_{HH}$ = 7.5 Hz, H6/6′), 7.32 (d, 4H, $^3J_{HH}$ = 6.9 Hz, H3/3′), 7.13 (t, 4H, $^3J_{HH}$ = 7.3 Hz, H5/5′), 6.94 (t, 4H, $^3J_{HH}$ = 7.1 Hz, H4/4′), 3.24 (s, 12H, Me_4N^+); HR ESI-MS (MeCN): calcd for $C_{24}H_{16}FSi^-$: 351.10108, found: 351.10081.

1-Bromo-[2]naphthylamine (9).[36] Finely ground β-naphthylamine (1.26 g, 8.8 mmol) and NBS (1.73 g, 9.7 mmol) were sonicated in CCl_4 (26.5 mL) under mechanical stirring. The reaction was followed by TLC (9:1 pentane/ethyl acetate). After 2 h, the dark-brown mixture was washed with water (2 × 20 mL), and the aqueous phase was extracted with DEE (20 mL). The aqueous phase was treated with 5% aqueous sodium bicarbonate (3 mL) and extracted again with DEE (20 mL). The organic layers were combined, dried on sodium sulfate, and evaporated to dryness. The crude black product was purified by column chromatography over silica gel eluting with 5:1 pentane/ethyl acetate. Subsequent crystallization from pentane afforded **9** as a faintly pink solid (1.33 g, 6.0 mmol, 69%). Mp: 59.8−60.9 °C; ^{13}C{^{1}H} NMR (100.6 MHz, $CDCl_3$): δ 142.2 (CNH_2), 133.2 (C8a), 128.75 (C4a), 128.72 (C4), 128.2 (C5), 127.8 (C7), 125.0 (C8), 123.0 (C6), 117.8 (C3), 104.2 (CBr); ^{1}H NMR (250.1 MHz, $CDCl_3$): δ 8.05 (dm, $^3J_{HH}$ = 8.5 Hz, 1H, H8), 7.69 (tdd, $^3J_{HH}$ = 8.1, $^4J_{HH}$ = 1.3, $^5J_{HH} \approx {}^4J_{HH4}$ = 0.7 Hz, 1H, H5), 7.62 (br d, $^3J_{HH}$ = 8.7 Hz, 1H, H4), 7.51 (ddd, $^3J_{HH}$ = 8.4, $^3J_{HH}$ = 6.9, $^4J_{HH}$ = 1.3 Hz, 1H, H7), 7.29 (ddd, $^3J_{HH}$ = 8.1, $^3J_{HH}$ = 6.9, $^4J_{HH}$ = 1.0 Hz, 1H, H6), 7.00 (d, $^3J_{HH}$ = 8.7 Hz, 1H, H3), 4.37 (br s, 2H, NH_2); R_f (silica/9:1 pentane/ethyl acetate): 0.3.

1-(1-Bromo-[2]naphthyl)-1H-pyrrole (10). 2,5-Dimethoxytetrahydrofuran (0.90 mL, 6.9 mmol) was added dropwise to a refluxing mixture of **9** (1.43 g, 6.45 mmol) in glacial acetic acid (5.0 mL). After 15 min, TLC (1:1 DCM/pentane) indicated complete conversion. At room temperature, the dark brown mixture was diluted with DCM (20 mL) and water (10 mL), and neutralized with 5% aqueous sodium bicarbonate. After extraction and washing with water, the combined aqueous layers were extracted with DCM. The combined organic layers were dried on magnesium sulfate and evaporated to dryness. Purification by column chromatography over silica gel eluting with 1:1 DCM/pentane afforded **10** as a yellow oil (1.53 g, 5.62 mmol, 87%). ^{13}C{^{1}H} NMR (100.6 MHz, $CDCl_3$): δ 138.5 (C2′), 133.5 (C4a′), 132.8 (C8a′), 128.6 (C4′), 128.34 (C5′/7′), 128.32 (C7′/5′), 128.2 (C8′), 127.2 (C6′), 125.9 (C3′), 122.7 (NCH), 120.1 (C1′), 109.3 (NC=*C*H); ^{1}H NMR (250.1 MHz, $CDCl_3$): δ 8.39 (d, $^3J_{HH}$ = 8.5 Hz, 1H, H8′), 7.90 (br d, $^3J_{HH}$ = 8.0 Hz, 1H, H5′), 7.87 (d, $^3J_{HH}$ = 8.5 Hz, 1H, H4′), 7.68 and 7.60 (ABMX, $^3J_{H7'H8'}$ = 8.5, $^3J_{H6'H5'}$ = 8.0, $^3J_{H6'H7'}$ = 6.9, $^4J_{H7'H5'}$ = 1.5, $^4J_{H6'H8'}$ = 1.3 Hz, 2H, H7′ and H6′), 7.45 (d, $^3J_{HH}$ = 8.6 Hz, 1H, H3′), 6.97 (t, $^3J_{HH}$ = 2.2 Hz, 2H, NCH), 6.40 (t, $^3J_{HH}$ = 2.2 Hz, 2H, NC=CH); HR EI-MS: calcd for $C_{14}H_{10}NBr$: 270.9997, found: 270.9988; *m/z*: 271 (100) $[M - {}^{79}Br]^+$, 273 (92) $[M - {}^{81}Br]^+$, 191 (26) $[M - HBr]^+$; R_f (silica/1:1 DCM/pentane): 0.8.

Bis([2]naphthylpyrrol-1′,2-diyl)silane (11). *n*-Butyllithium (7.0 mL, 11.1 mmol) was added dropwise to **10** (1.506 g, 5.53 mmol) in DEE (10.0 mL) at 0 °C, and the resulting yellow suspension was stirred for 2 h. Tetrachlorosilane (317 μL, 2.77 mmol) was added, and the stirred mixture was allowed to warm to room temperature overnight. The resulting bright-yellow suspension was quenched with water, diluted with DEE (50 mL) and slightly acidified water (50 mL), and the phases were separated. The aqueous layer was extracted with DEE, and the combined organic layers were washed with water and dried on magnesium sulfate. After evaporation of the solvent, the crude brown product was purified by column chromatography over silica gel eluting with 5:1 pentane/DEE to afford a khaki-yellow powder (0.96 g, 2.34 mmol, 85%). Mp 218.7−223.2 °C, dec; ^{1}H,^{29}Si ge-HMBC NMR (400.1 MHz, $CDCl_3$): δ −36; ^{13}C APT NMR (100.6 MHz, $CDCl_3$): δ 147.9 (C2′), 137.5 (C8a′), 133.6 (C4′), 131.3 (C4a′), 128.7 (C5′), 127.8 (C7′), 127.6 (C8′), 124.8 (C6′), 123.7 (C2), 121.6 (C3), 119.8 (C5), 119.2 (C1′), 114.3 (C4), 112.8 (C3′); ^{1}H NMR (400.1 MHz, $CDCl_3$): δ 8.02 (d, $^3J_{HH}$ = 8.8 Hz, 2H, H4′), 7.76 (br d, $^3J_{HH}$ = 8.2 Hz, 2H, H5′), 7.73 (d, $^3J_{HH}$ = 8.8 Hz, 2H, H3′), 7.71 (dd, $^3J_{HH}$ = 2.7, $^4J_{HH}$ = 0.7 Hz, 2H, H3), 7.23 and 7.18 (br) and 7.13 (ABCX, $^3J_{H6'H5'}$ = 8.1, $^3J_{H7'H8'}$ = 7.9, $^3J_{H6'H7'}$ = 6.8, $^4J_{HH}$ = 1.4, $^4J_{HH}$ = 1.1 Hz, 6H,

H6′ and H8′ and H7′), 6.63 (dd, $^3J_{HH}$ = 3.3, $^4J_{HH}$ = 0.7 Hz, 2H, H3), 6.49 (dd, $^3J_{HH}$ = 3.3, $^3J_{HH}$ = 2.7 Hz, 2H, H4); HR EI-MS: calcd for $C_{28}H_{18}N_2Si$: 410.1239, found: 410.1249; *m*/*z*: 410 (100) $[M]^+$.

Lithium Methylbis([2]naphthylpyrrol-2,1′-diyl)silicate (6). In an NMR tube under N_2, **11** (56 mg, 136 μmol) was dissolved in THF (1.0 mL). Methyllithium (90 μL, 144 μmol) was added at −78 °C. The tube was capped airtight, and the yellow mixture was slowly warmed to room temperature while vortexing. NMR measurements were performed without lock; the magnetic field was shimmed visually on the ^{1}H FID signal.[43] ^{1}H,^{29}Si ge-HMBC NMR (400.1 MHz, THF): δ −129; ^{13}C{^{1}H} NMR (100.6 MHz, THF): δ 153.2 (C1′), 141.8 (C2′), 139.7 (C8a′), 138.9 (C2), 132.7 (C8′), 131.8 (C4a′), 127.7 (C5′), 125.3 (C4′), 122.7 (C7′), 121.6 (C6′), 120.5 (C3), 113.2 (C5), 111.8 (C3′), 110.1 (C4), 8.4 (Me); ^{1}H NMR (400.1 MHz, THF): δ 8.41 (br d, $^3J_{HH}$ = 8.1 Hz, 2H, H8′), 7.62 (dd, $^3J_{HH}$ = 7.5, $^4J_{HH}$ = 1.7 Hz, 2H, H5′), 7.49 and 7.47 (AB, $^3J_{HH}$ = 8.2 Hz, 4H, H4′ and H3′), 7.29 (br s, 2H, H5), 7.12 and 7.09 (ABMX, $^3J_{H7'H8'}$ = 8.1, $^3J_{H6'H5'}$ = 7.5, $^3J_{H6'H7'}$ = 7.0, $^4J_{H7'H5'}$ = 1.7,$^4J_{H6'H8'}$ = 1.5 Hz, 2H, H7′ and H6′), 5.95 (dd, $^3J_{HH}$ = 3.1, $^3J_{HH}$ = 2.4 Hz, 2H, H4), 5.78 (br s, 2H, H3), 0.68 (s, 3H, Me); HR EI-MS (200 °C): calcd for $C_{29}H_{22}N_2Si$ (M + H): 426.1552, found: 426.1552; *m*/*z*: 426 (100) $[M + H]^+$, 411 (58) $[M + H - Me]^+$, 193 (61) $[NaphPyr]^+$.

Lithium Ethylbis(phenylpyrrol-2,2′-diyl)silicate (12). Bis(phenylpyrrol-2,2′-diyl)silane (42.3 mg, 136 μmol) in THF-d_8 (0.5 mL) was treated with ethyllithium (272.5 μL, 136.3 μmol) at −78 °C under N_2. The pale-yellow mixture was slowly warmed to room temperature, and all volatiles were evaporated under reduced pressure. The crude residue was analyzed by NMR spectroscopy in THF-d_8. ^{1}H,^{29}Si ge-HMBC NMR (400.1 MHz, THF-d_8, 223 K): δ −124.9; ^{1}H,^{13}C HSQC and HMBC NMR (400.1 MHz, THF-d_8, 223 K): δ 155.7 (q, C2′), 146.1 (q, C1′), 139.5 (q, C2), 133.9 (C3′), 124.4 (C5′), 122.1 (C4′), 119.7 (C3), 113.7 (C5), 110.6 (C4), 109.3 (C6′), 16.1 (CH_2), 11.6 (CH_3); ^{1}H NMR (400.1 MHz, THF-d_8, 223 K): δ 7.61 (dd, $^3J_{HH}$ = 6.6, $^4J_{HH}$ = 1.2 Hz, H3′), 7.28 (dd, $^3J_{HH}$ = 2.4, $^4J_{HH}$ = 1.3 Hz, H5), 7.12 (d, $^3J_{HH}$ = 7.6 Hz, H6′), 6.94 and 6.86 (ABMX, $^3J_{H5'H6'}$ = 7.8, $^3J_{H4'H5'}$ = 7.2, $^3J_{H4'H3'}$ = 6.8, $^4J_{H5'H3'}$ = 1.5, $^4J_{H4'H6'}$ = 1.1 Hz, H5′ and H4′), 6.15 (dd, J = 3.0, 1.2 Hz, H3), 6.05 (dd, J = 2.9, 2.5 Hz, H4), 0.94 and 0.78 and 0.76 (AB_3C, $^2J_{H^{ax}H^{eq}}$ = −13, $^3J_{H^{eq}H} \approx {}^3J_{H^{ax}H}$ = 8 Hz, H^{eq}, CH_3 and H^{ax}).

Lithium Ethylbis([2]naphthylpyrrol-2,1′-diyl)silicate (13). Bis([2]naphthylpyrrol-2,2′-diyl)silane (43.1 mg, 105 μmol) in THF-d_8 (0.5 mL) was treated with ethyllithium (210.0 μL, 105.0 μmol) at −78 °C under N_2. The orange mixture was slowly warmed to room temperature, and all volatiles were evaporated under reduced pressure. The crude yellow residue was analyzed by NMR spectroscopy in THF-d_8. ^{1}H,^{29}Si ge-HMBC NMR (400.1 MHz, THF-d_8): δ −121.5; ^{13}C APT NMR (100.6 MHz, THF-d_8): δ 153.7 (q, C1′), 143.3 (q, C2′), 140.7 (q, C8a′), 139.2 (q, C2), 133.5 (C8′), 132.6 (q, C4a′), 128.6 (C5′), 126.2 (C4′), 123.6 (C7′), 122.4 (C6′), 121.8 (C3), 114.2 (C5), 112.5 (C3′), 110.8 (C4), 16.3 (CH_2), 10.3 (CH_3); ^{1}H NMR (400.1 MHz, THF-d_8): δ 8.46 (br d, $^3J_{HH}$ = 8.2 Hz, H8′), 7.67 (dd, $^3J_{HH}$ = 8.0, $^4J_{HH}$ = 1.3 Hz, H5′), 7.53 and 7.50 (AB, $^3J_{HH}$ = 8.5 Hz, H4′ and H3′), 7.33 (dd, $^3J_{HH}$ = 2.2, $^4J_{HH}$ = 1.3 Hz, H5), 7.18 and 7.13 (ABMX, $^3J_{H7'H8'}$ = 8.2, $^3J_{H6'H5'}$ = 8.0, $^3J_{H6'H7'}$ = 6.8, $^4J_{H7'H5'}$ = 1.3, $^4J_{H6'H8'} \approx$ 1 Hz, H7′ and H6′), 6.00 (dd, $^3J_{HH}$ = 3.0, $^3J_{HH}$ = 2.3 Hz, H4), 5.84 (dd, $^3J_{HH}$ = 3.1, $^4J_{HH}$ = 1.2 Hz, H3), 1.48 (dq, $^2J_{HH}$ = −13.5, $^3J_{HH}$ = 8 Hz, H^{eq}), 1.17 (dq, $^2J_{HH}$ = −13.6, $^3J_{HH}$ = 8 Hz, H^{ax}), 0.66 (t, $^3J_{HH}$ = 7.8 Hz, CH_3).

Acknowledgment. This work has been supported by The Netherlands Organization for Scientific Research, Chemical Sciences (NWO-CW). The National Center for Computing Facilities (SARA) is acknowledged for computer time. We thank Dr. M. Smoluch (VU University Amsterdam), J. W. H. Peeters (University of Amsterdam), and L. Bertschi (ETH Zürich) for the exact mass determinations.

Supporting Information Available: NMR spectra of reported compounds; estimation of epimerization barrier for **12**; diastereotopic proton assignment for **13**; description of tetrasiloxane; atomic coordinates and energies of all calculated structures, input for the PES scan, and complete ref.[16] This material is available free of charge via the Internet at http://pubs.acs.org.

JA809154G

(43) Hoye, T. R.; Eklov, B. M.; Ryba, T. D.; Voloshin, M.; Yao, L. J. *Org. Lett.* **2004**, *6*, 953–956.